Chinese Chemical Letters 33 (2022) 3909–3915

Contents lists available at ScienceDirect

Chinese Chemical Letters

journal homepage: www.elsevier.com/locate/cclet

An integrated approach to configure rGO/VS_4/S composites with improved catalysis of polysulfides for advanced lithium–sulfur batteries

Feng Li[a,1], Lu Wang[b,1], Guangmeng Qu[a], Peiyu Hou[a,*], Linglong Kong[c,*], Jinzhao Huang[a], Xijin Xu[a,*]

[a] School of Physics and Technology, University of Jinan, Ji'nan 250022, China
[b] College of Chemistry and Material Science, Shandong Agricultural University, Taian 271018, China
[c] State Forestry and Grassland Administration Key Laboratory of Silviculture in Downstream Areas of the Yellow River, School of Forestry, Shandong Agricultural University, Taian 271018, China

ARTICLE INFO

Article history:
Received 2 August 2021
Revised 8 September 2021
Accepted 14 November 2021
Available online 19 November 2021

Keywords:
Lithium–sulfur batteries
rGO/VS_4/S composites
In-situ synthesis
Adsorbing
Catalysis

ABSTRACT

Lithium–sulfur (Li–S) battery is labeled as a promising high-energy-density battery system, but some inherent drawbacks of sulfur cathode materials using relatively complicated techniques impair the practical applications. Herein, an integrated approach is proposed to fabricate the high-performance rGO/VS_4/S cathode composites through a simple one-step solvothermal method, where nano sulfur and VS_4 particles are uniformly distributed on the conductive rGO matrix. rGO and sulfiphilic VS_4 provide electron transfer skeleton and physical/chemical anchor for soluble lithium polysulfides (LiPS). Meanwhile, VS_4 could also act as an electrochemical mediator to efficiently enhance the utilization and reversible conversion of LiPS. Correspondingly, the rGO/VS_4/S composites maintain a high reversible capacity of 969 mAh/g at 0.2 C after 100 cycles, with a capacity retention rate of 82.3%. The capacity fade rate could lower to 0.0374% per cycle at 1 C. Moreover, capacity still sustains 795 mAh/g after 100 cycles in the relatively high-sulfur-loading battery (6.5 mg/cm^2). Thus, the suggested method in configuring the sulfur-based composites is demonstrated a simple and efficient strategy to construct the high-performance Li–S batteries.

The rapidly developing society has aroused more demands on high-energy-density storage systems, especially with the springing up of smart electronics, electric vehicles, and available clean energy [1,2]. Traditional secondary batteries, such as lead-acid battery, nickel-chromium battery and lithium-ion battery, are stuck in the limited theoretical capacity of electrode materials [3,4]. Lithium–sulfur (Li–S) battery is considered as a powerful competitor by virtue of employing high capacity electrodes (3860 mAh/g_{Li} and 1675 mAh/g_S). The merits of sulfur, including abundant resource, economic cost and low toxicity, further guarantee its good application prospect [5]. However, the practical process of Li–S battery has been seriously impeded by some existing obstacles. The inherently insulative property of sulfur and reduced products (Li_2S_2/Li_2S), the uncontrollable diffusion of soluble lithium polysulfides (LiPS), and the distinct volume fluctuation during the mutual transformation between S and Li_2S are included [6]. These knotty issues could induce unstable sulfur electrode with underutilized active materials, low coulombic efficiency and obvious structure variation, insecure lithium metal anode, and even battery failure [7,8].

Massive researches have been concentrated on fabricating high-performance sulfur cathode by introducing different kinds of functional host materials. Carbonaceous material with flourishing pore structure and good electron conductivity is a common choice to physically restrict the LiPS and maintain stable electrochemical performance [9–12]. But the weak physical interaction seems insufficient to guarantee electrochemical stability [13]. Thus, heteroatom-doped carbons [14,15] and polar compounds (*e.g.*, metal oxides [16–18], metal nitrides [19], metal sulfides [20–22], metal carbides [23], metal-organic frameworks [24], organic compounds [25]) have been applied to enhance the interaction with LiPS by chemical adsorption, and improve the reaction kinetics by electrocatalysis [26–29]. However, the limited conductivity of most polar materials would partly impede the redox reactions and impair the electrochemical stability of sulfur cathode, espe-

* Corresponding authors.
E-mail addresses: sps_houpy@ujn.edu.cn (P. Hou), linglongkong@mail.nankai.edu.cn (L. Kong), sps_xuxj@ujn.edu.cn (X. Xu).
[1] These authors contributed equally to this work.

https://doi.org/10.1016/j.cclet.2021.11.046
1001-8417/

cially under high current density and sulfur loading. Thus, conductive carbon skeletons are always synergistically employed with polar materials to ensure the sufficient utilization of sulfur [30–32]. The exploration of high-efficiency host materials and the structural design of the sulfur cathode are becoming the consensuses on lifting the performance of Li–S battery. Moreover, the benign contact of sulfur with the host materials is another important factor to ensure the electrochemical performance of sulfur cathode. However, sulfur agglomeration and the induced poor contact with host materials are often occurred in the traditional preparation methods [33–39], which may be adverse to the utilization of sulfur and the cyclic performance of Li–S battery. Therefore, preparing sulfur-based composites by coupling the polar substances with carbon skeletons and elemental sulfur in a simple and integrated method is preferable for fabricating the high-performance Li–S battery.

Herein, for the first time, rGO/VS_4/S composites are successfully prepared through the one-step solvothermal method. By innovatively adding H_2O_2 oxidant, VS_4 and S nanoparticles could be in-situ generated on rGO matrix during the chemical reactions and self-assembly processes, accompanied by their uniform distribution and benign contact. The corresponding preparation period and cost are drastically reduced. rGO with a typical two-dimension structure and high surface area is selected as a matrix due to the good electrical conductivity and abundant active sites for electrochemical reactions, as well as the controlled chemical composition or morphology regulation on the decorated polar materials [40,41]. VS_4, as a kind of the polar transitional metal dichalcogenides, possesses the typical one-dimension chain structure [42,43], and has been recently applied as electrochemically active materials in some secondary battery systems [44–48]. The unique interaction between the adjacent $V^{4+}(S_2^{2-})_2$ chains with weak van der Waals forces are expected to facilitate the fast charge transfer and enhance the anchoring of LiPS in Li–S battery [49]. The obtained VS_4 combined with rGO could provide satisfying conductivity and sufficient electrocatalytic sites for the electrochemical reaction of sulfur. Moreover, the adopted one-step synthetic technique contributes to a uniform distribution of sulfur and a commendable contact between the hosts and sulfur. Thus the corresponding capacity of the Li–S battery could be 1177 mAh/g at 0.2 C, and maintains 969 mAh/g after 100 cycles. The capacity decay rate is as low as 0.0374% per cycle at 1 C during the 1000 cycles. Meanwhile, the high sulfur loading electrode ($\sim$6.5 mg/cm^2) also delivers the enhanced cyclic performance and rate capability.

As shown in Fig. 1a, rGO/VS_4/S composites are constructed via the one-pot hydrothermal method. The well-dispersed GO could act as the reaction location and morphology mediator for the sulfur and VS_4 along with its reduction in rGO. The soluble CH_3CSN_2, Na_3VO_4 and H_2O_2 may undergo a series of chemical reactions, as listed in Fig. 1a. Consequently, VS_4 and S are simultaneously in-situ generated on the lamellar rGO substrates. In general, VS_4 is directly synthesized through the reaction between metal V and S powders, or between CH_3CSN_2 and Na_3VO_4 [42,50], then elemental S or liquid sulfur species are introduced to fabricate the active materials for Li–S battery through multi-step or complicated procedures in the published works of literature [42,49]. The method we proposed employs H_2O_2 as reactant to oxide S^{2-} and S_2^{2-}, accompanied by the synchronous generation of S and VS_4, which could guarantee the simple preparation process, the uniform distribution and favorable contact of sulfur and polar hosts. The SEM image confirms the porous aggregated morphology of rGO/VS_4/S composites (Fig. 1b), combined with the uniform distribution of elemental S and V on the rGO matrix (Fig. S1 in Supporting information). The TEM image in Fig. 1c verifies the decoration of nano-sized sulfur and VS_4 particles on the rGO nanosheets. The HRTEM images (Fig. 1d) further affirm the decorated VS_4 with the typical lattice fringes of ($\bar{4}02$) plane. The corresponding interplanar spacing is 0.247 nm. Besides, the XRD pattern identifies the formation of orthorhombic α-S_8 (JCPDS No. 08–0247) [51] and monoclinic VS_4 (JCPDS No. 21–1434) [52] in the obtained composites (Fig. 1e). Moreover, the applied XPS test demonstrates the feasibility of synthesizing rGO/VS_4/S composites through this simple and in-situ method. The V 2p spectrum in the rGO/VS_4/S composites shows the typical peaks of VS_4 at 517.18 eV ($2p_{3/2}$) and 524.56 eV ($2p_{1/2}$) (Fig. 1f) [42]. In the meantime, the characteristic peak of S_2^{2-} (162.74 eV) also validates the existence of VS_4 (Fig. 1g) [49]. Furthermore, the peaks located at 163.68 eV and 164.74 eV [53] in S 2p spectrum reveal the simultaneous generation of elemental sulfur during the hydrothermal reaction process. The rGO/S composites for comparison endow the similar assembled morphology with the homogeneous distribution of orthorhombic α-S_8 in Figs. S2 and S3a (Supporting information).

In addition, the content of elemental V in the rGO/VS_4/S composites is confirmed by the ICP test, which is 2.05 wt%. Accordingly, the mass ratio of VS_4 is calculated to be 7.2 wt%. TG results reveal the weight loss of rGO/VS_4/S composites below 300 °C is 83.2 wt% (Fig. S3b in Supporting information), including the evaporation of S and the transformation from VS_4 to VS_x ($2 < x < 3$) [54]. The corresponding S content is calculated to 81.2 wt% by deducting the mass decrement of VS_4, and then 11.6 wt% rGO is included in the as-prepared rGO/VS_4/S composites. While the contrast sample of rGO/S composites consists of 78.7 wt% S and 21.3 wt% rGO. The above results illustrate that VS_4 and S nanoparticles could be simultaneously formed on the rGO matrix with benign contact and homogeneous distribution, which may avail to enhance the interaction between host materials and LiPS, and the utilization of active materials. The proposed method is proved to be an available strategy to fabricate the integrated cathode materials for Li–S battery during the *in-situ* self-assembled process.

The practical effect of the host materials on the soluble LiPS is firstly examined by soaking rGO/VS_4 and rGO in the Li_2S_4, Li_2S_6 and Li_2S_8 solution, respectively. The relevant results after 1 h adsorption demonstrate the outstanding LiPS adsorptivity of rGO/VS_4 in contrast to rGO hosts, accompanied by the rapid and distinct color fading (Fig. 2a). Moreover, the theoretical calculation based on DFT is carried out to evaluate the adsorption behavior of VS_4 on LiPS. (110) plane of VS_4 is selected to interact with different LiPS species. The optimizedadsorption structure and calculated binding energies corresponding to VS_4 and Li_2S_4, Li_2S_6 and Li_2S_8 are -2.3 eV, -1.5 eV and -1.8 eV, respectively (Figs. 2b and c). These values are much larger than that of carbon hosts (0.39$\sim$0.61 eV) [55], and nearly equivalent to the values of other polar metal compounds [56]. The increased binding energy indicates the enhanced adsorption capability on LiPS owing to the structural characters of VS_4. Thus the prepared rGO/VS_4 host materials are proved to effectively anchor the LiPS by introducing VS_4 nanoparticles, which may exert a positive effect on the following conversion processes.

Subsequently, symmetric cells including two rGO or rGO/VS_4 identical electrodes, and Li_2S_6-free or Li_2S_6-containing solution (0.5 mol/L) as electrolyte are configured to investigate the catalytic effect on LiPS. CV technique is applied to test the redox conversion of LiPS. The cells without Li_2S_6 display an ignorable current both in rGO and rGO/VS_4 systems (Figs. 2d and e), indicating a minor contribution by the capacitive current. Then the peak currents of Li_2S_6-containing cells are closely related to the redox process of Li_2S_6. The peak in the cathodic process reflects the reduction reaction from Li_2S_6 to Li_2S, and the anodic peak is associated with the reversible conversion from Li_2S to Li_2S_6, even to sulfur [57]. The symmetric cell using rGO/VS_4 electrode exhibits more distinct peaks and higher peak currents compared with the cell solely adopting rGO electrode. In detail, the rGO materials induce to the broadened peaks with the enlarged peak separation, corresponding to the poor electrochemical kinetics and reversibility.

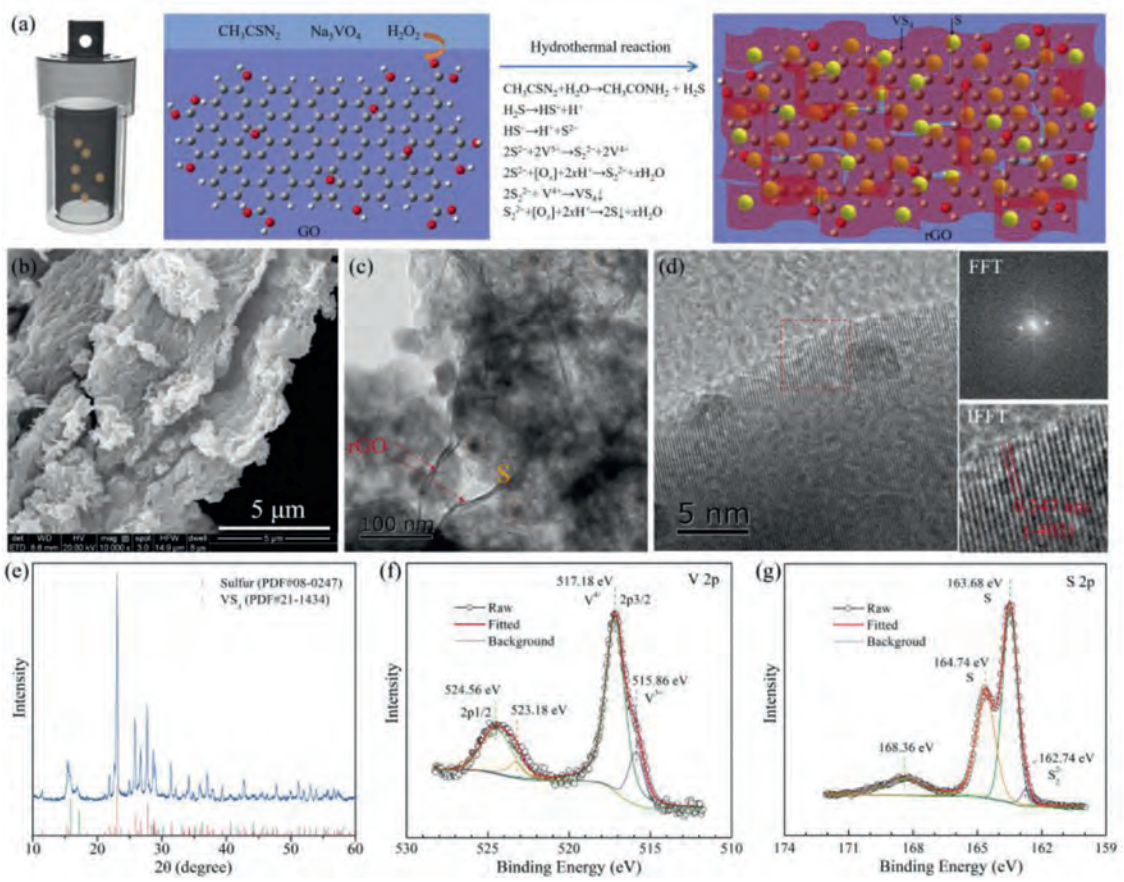

Fig. 1. (a) Schematic illustration of one-pot, *in-situ* synthesis of rGO/VS_4/S composites *via* hydrothermal reactions. (b) SEM, (c, d) TEM, (e) XRD and (f, g) XPS spectra of the as-prepared rGO/VS_4/S composites.

Instead, rGO/VS_4 facilitates the occurrence of the sharp and adjacent peaks, indicating the enhanced catalysis on LiPS. Meanwhile, almost the same CV curves are obtained in the continuous test for rGO/VS_4 cells, demonstrating the boosted electrochemical stability during the redox reactions. Furthermore, the Li^+ diffusion coefficient ($D_{Li}{}^+$) could be calculated by the Randles-Sevick equation according to the CV results at 5, 10 and 20 mV/s, and the relevant fitting results (Fig. S4 in Supporting information) [36]. The values of $D_{Li}{}^+$ in the cathodic and anodic processes are 1.59×10^{-8} cm^{-2} s^{-1} and 1.93×10^{-8} cm^{-2} s^{-1}, respectively. These values are much higher than that of the reference Li–S cells ($\sim 10^{-9}$ cm^{-2} s^{-1}) [58]. The increased Li^+ diffusion coefficient corresponds to the facilitated charge-transfer behavior during the electrochemical conversion. The above theoretical and experimental results validate that the prepared rGO/VS_4 hosts endow the enhanced adsorptivity on LiPS and the improved redox kinetics, which could contribute to the electrochemical performance of Li–S battery.

Then the electrochemical performance of Li–S cells utilizing rGO/S and rGO/VS_4/S cathodes is detailedly studied. First, the employed CV tests show similar redox characteristics in 1.5∼2.8 V (*vs.* Li/Li^+), which are the same as the conventional Li–S cell, except for the potential difference (Fig. 3a). The Li–S cell with rGO/VS_4/S has a relatively small potential difference during the cathodic/anodic processes, indicating the enhanced kinetics and the reduced polarization. The small reduction peak at ∼1.8 V (*vs.* Li/Li^+) may be ascribed to the transformation from VS_4 to Li_xVS_4 [54]. The discharge-charge curves (Figs. 3b and c) further reveal the improved reaction kinetics of rGO/VS_4/S cathode with the smaller potential difference (118 mV *vs.* 157 mV), larger capacity (1362 mAh/g *vs.* 1276 mAh/g) and better stability at 0.1 C. Second, the cycle performance at 0.2 C occurs the obvious difference (Fig. 3d). The cell with rGO/S cathode endows the inferior capacity and fast capacity fade. The capacity decreases from 1045 mAh/g to 409 mAh/g with a retention rate of 39.1% after 100 cycles. As contrast, the rGO/VS_4/S-containing cell delivers a high capacity (1362 mAh/g in the first cycle) and the enhanced cycle stability. The capacity retention rate could sustain 82.3% with a capacity of 969 mAh/g after 100 cycles. The related discharge-charge curves after certain cycles (Figs. 3e and f) also demonstrate the improved electrochemical performance by adopting rGO/VS_4/S, with well-maintained plateaus, reduced polarization, and relatively stable capacity. These results imply that simple physical confinement by rGO is seemingly insufficient to restrict the LiPS and ameliorate their electrochemical conversion. The effective entrapment and adequate utilization of LiPS could be simultaneously achieved in the cell with rGO/VS_4/S. Third, the superiority of rGO/VS_4/S electrode is also reflected in the long-term cycling at 1 C. As shown in Fig. 3g, the capacity reaches 880 mAh/g, and maintains 548 mAh/g after 1000 cycles with a capacity retention rate of 62.6%. The fade rate could lower to 0.0374% per cycle, which is smaller than that of some reported works [36].

Redox plateaus are well retained with the nearly unchanged polarization potential (Fig. S5a in Supporting information), exhibiting the outstanding ability of rGO/VS_4 in preserving the cyclic stabilization of Li–S battery. Forth, rate capability is another evidence to prove the advantage of rGO/VS_4/S from 0.1 C to 5 C (Fig. 3h). The average capacity of rGO/VS_4/S could reach 1338 mAh/g, 1163 mAh/g, 996 mAh/g, 869 mAh/g, 730 mAh/g and 507 mAh/g, respectively, at 0.1 C, 0.2 C, 0.5 C, 1 C, 2 C and 5 C. In comparison, the corresponding capacity value of rGO/S at the same rate

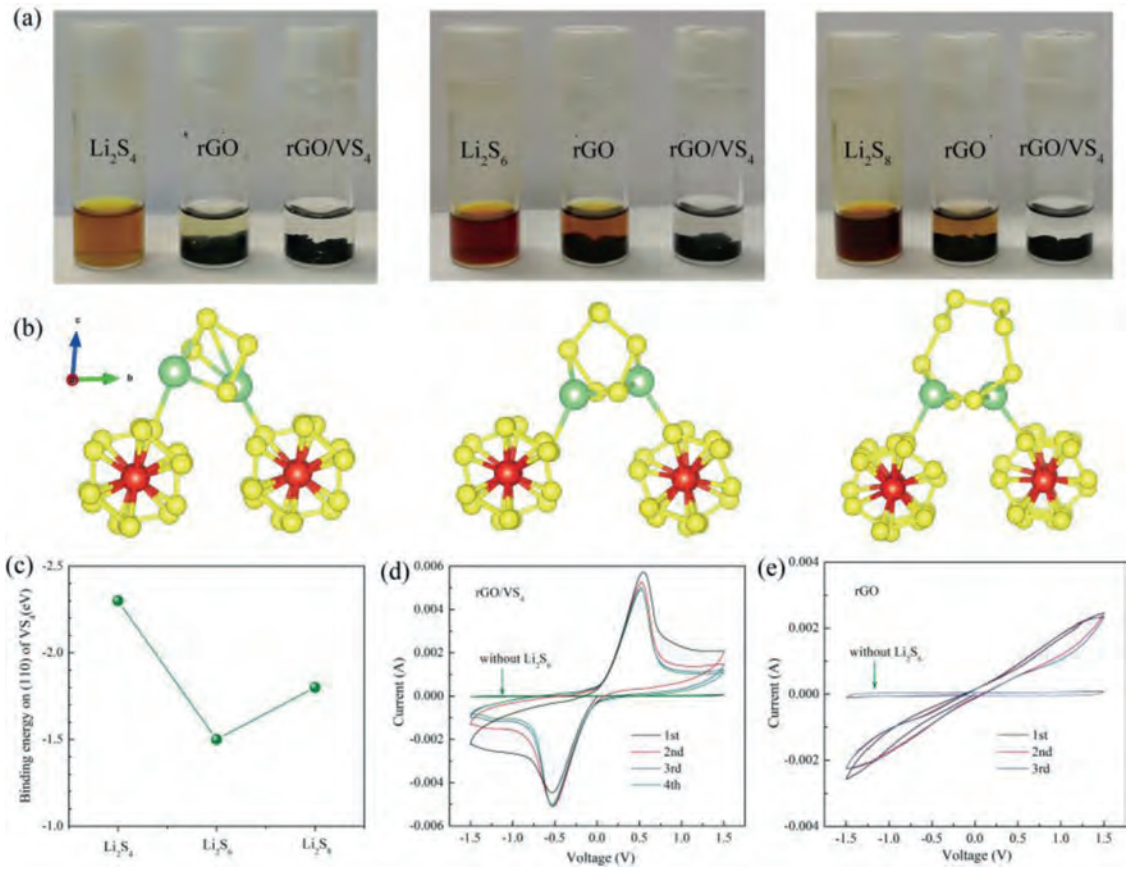

Fig. 2. (a) Adsorption test of LiPS (Li_2S_4, Li_2S_6, Li_2S_8) on rGO and rGO/VS_4. (b, c) The optimized adsorption structure and calculated binding energies between LiPS and (110) plane of VS_4 (S atom in yellow, V atom in red and Li atom in green). CV curves of (d) rGO/VS_4 and (e) rGO symmetric cells with and without Li_2S_6.

is small. The related discharge-charge profiles further illustrate the enhancement of rGO/VS_4/S on charge transfer and redox reactions with the enlarged plateau area and the reduced polarization (Figs. S5b and c in Supporting information).

Furthermore, the electrochemical performance of rGO/VS_4/S-containing cells with different sulfur loadings (~3.0 mg/cm^2 and ~6.5 mg/cm^2) is also evaluated. Although the redox potential difference is slightly aggrandized from 136 mV to 176 mV with the increase of sulfur loading, the cells show the same discharge-charge characteristics (Fig. 3i). The reversible capacity at 0.1 C could be 1274 mAh/g and 1174 mAh/g, respectively, indicating a relatively sufficient utilization of sulfur even under high sulfur loading. The cells deliver the initial capacity of 1099 mAh/g and 987 mAh/g at 0.2 C, respectively. The corresponding capacity retention rate could be 79.6% and 81.5%, respectively, with the reversible capacity of 875 mAh/g and 803 mAh/g after 100 cycles (Fig. 3j). Meanwhile, the cells display superior rate capability from 0.1 C to 2 C in Fig. 3k and Fig. S5d (Supporting information). Typically, the capacity of the cell with a sulfur loading of 6.5 mg/cm^2 reaches 457 mAh/g at 2 C. Thus the positive effect of rGO/VS_4 could also extend to the high-loading Li–S cells, which may promote the process of Li–S cells in the practical application level [59–61].

The above results show the positive role of the synthesized host materials in enhancing the electrochemical availability and stability of Li–S cells, and the relevant mechanism could be properly clarified through the following characterizations. The as-prepared rGO and rGO/VS_4 could deliver certain capacity contributions, especially rGO/VS_4 in the given potential range in Fig. S6a (Supporting information), which is similar to the previous reports [58,62]. The capacity could stabilize at ~300 mAh/g, which contributes ~70 mAh/g to the capacity of the rGO/VS_4/S. The pristine VS_4 in the rGO/VS_4/S could convert into Li_2VS_4 (PDF#34–0790) or $Li_{3+x}VS_4$ ($0 \leq x$) [51] during the discharged process (Fig. S6b in Supporting information), and exerts the relatively enhanced interaction with LiPS, and the recover after recharging. The discharged rGO/VS_4 electrode in the adsorption experiment (Fig. S6c in Supporting information) exerts the relatively enhanced interaction with LiPS, and corresponding characteristic diffraction peaks occur obvious shifts to high angle (Fig. S6d in Supporting information), which may signify the Li^+ transfer from the lithiated hosts to LiPS, as demonstrated in the reported $Nb_{18}W_{16}O_{93}$ [29] and Mo_6S_8 [63] hosts. Thus, VS_4 combined with its lithiated intermediates could act as a chemical anchor and Li^+/electrons mediator for LiPS conversion, and the rGO matrix assists the chemical/catalytic interaction with benign conductivity and mechanical property [11,64].

Additionally, the corresponding EIS curves of the cycled Li–S cells at 0.2 C (Fig. 4a) imply why the rGO/VS_4/S cell endows such excellent electrochemical performance. The obtained curves are fitted by using the given equivalent circuit in Fig. S7 (Supporting information), and the relevant results are exhibited in Table S1 (Supporting information). The corresponding surficial layer resistance (Rs in the high-frequency area, 53.6 Ω), charge-transfer resistance (R_{ct} in the medium-frequency region, 49.2 Ω) and semi-infinite diffusion impedance (W_o in the low-frequency interval, 67.2 Ω) of the rGO/VS_4/S cell with small values demonstrate the facilitated charge transfer during the repeated redox conversions. In the meantime, analysis of the disassembled cells after 100 cycles at 0.2 C provides more information. SEM and EDS images on the cycled rGO/S electrode show the excessive aggregation of active materials on the outside of rGO hosts in Fig. 4b and Fig. S8a (Supporting information), leading to the architecture failure or even invalidation of the

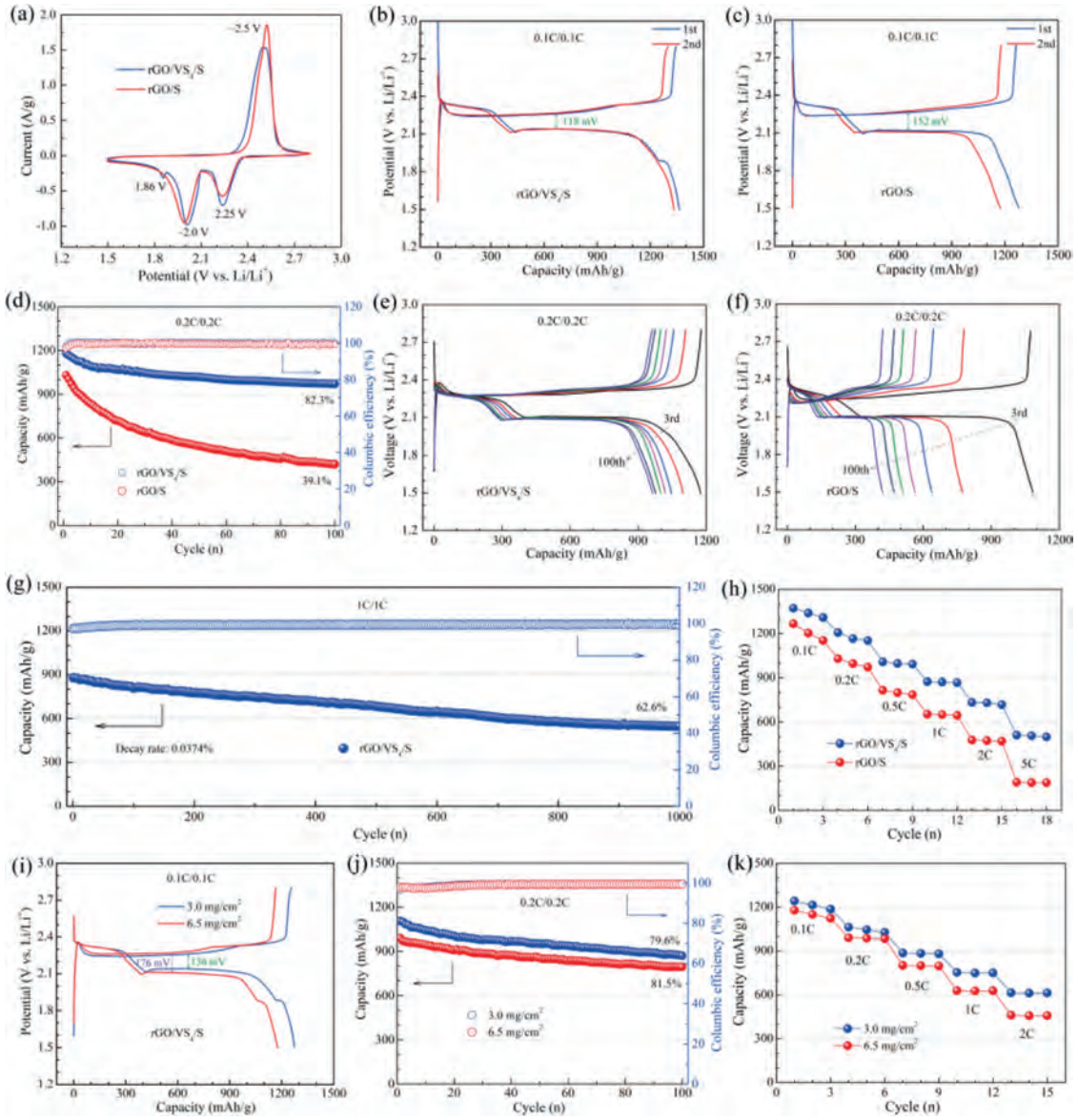

Fig. 3. Comparison of electrochemical properties for the rGO/S and rGO/VS_4/S composites: (a) CV curves. (b, c) The initial two charge/discharge curves at 0.1 C. (d-g) cycling life at 0.2 C and 1 C. (h) Comparison of rate performance for the rGO/S and rGO/VS_4/S composites. (i-k) The electrochemical properties for the rGO/VS_4/S composites with varied S loadings.

physical entrapment. While rGO/VS_4/S could restrain the surface deposition and sustain the configuration (Fig. 4c and Fig. S8b in Supporting information), which may guarantee the electrochemical stabilization. As expected, the cycled rGO/VS_4/S electrode has fewer free LiPS compared to the cycled rGO/S electrode, accompanied by the light-colored soaking solution and negligible characteristic peaks of LiPS (Fig. 4d). The strong adsorption peak located at ~280 nm corresponds to the long-chain soluble LiPS (S_6^{2-}) from the reduction reaction of S_8 [29,65]. The reduction of dissociative LiPS in the rGO/VS_4/S electrode reflects their effective confinement and sufficient conversion. The tested XPS spectra further validate the existence of elemental sulfur in the cycled rGO/VS_4/S electrode with the obvious characteristic peaks at 163.46 eV and 164.72 eV (Fig. 4f). Clearly, rGO/VS_4/S electrode possesses more elemental S in contrast with the rGO/S electrode (Fig. 4e), indicating the enhanced electrochemical reversibility by employing the *in-situ* self-assembled rGO/VS_4/S composites. The $NS^*O_2CF_3$ bond may be ascribed to the residual of Li salts, while the $-SO_4$ and $-SO_3$ may be related to the products from the reaction between LiPS and $LiNO_3$ [66], and the momentary air contact during the samples preparing and transferring process [67].

Therefore, the relevant results from the structure and electrochemical performance analysis jointly demonstrate that the rGO/VS_4/S composites via one-step hydrothermal treatment are contributed to enhance the reliability and stability of Li–S battery by effectively trapping the soluble LiPS and catalyzing their reversible conversion. As shown in Fig. 5, the proposed method is easy to construct the rGO/VS_4/S configuration with the uniform distribution and well mutual contact of sulfur and VS_4 nanoparticles on rGO matrix. rGO and VS_4 could provide a benign conductive network to achieve fast electron transfer in the Li–S battery. Meanwhile, rGO supplies favorable physical restriction, and VS_4 offers strong chemical adsorption and catalysis on LiPS. Thus, the efficient and reversible conversion involving solid sulfur, soluble LiPS, and solid Li_2S could be fluently occurred, accompanied by the improved electrochemical reversibility and stability.

In summary, rGO/VS_4/S composites are simultaneously prepared during the in-situ assembling process in the one-step hydrother-

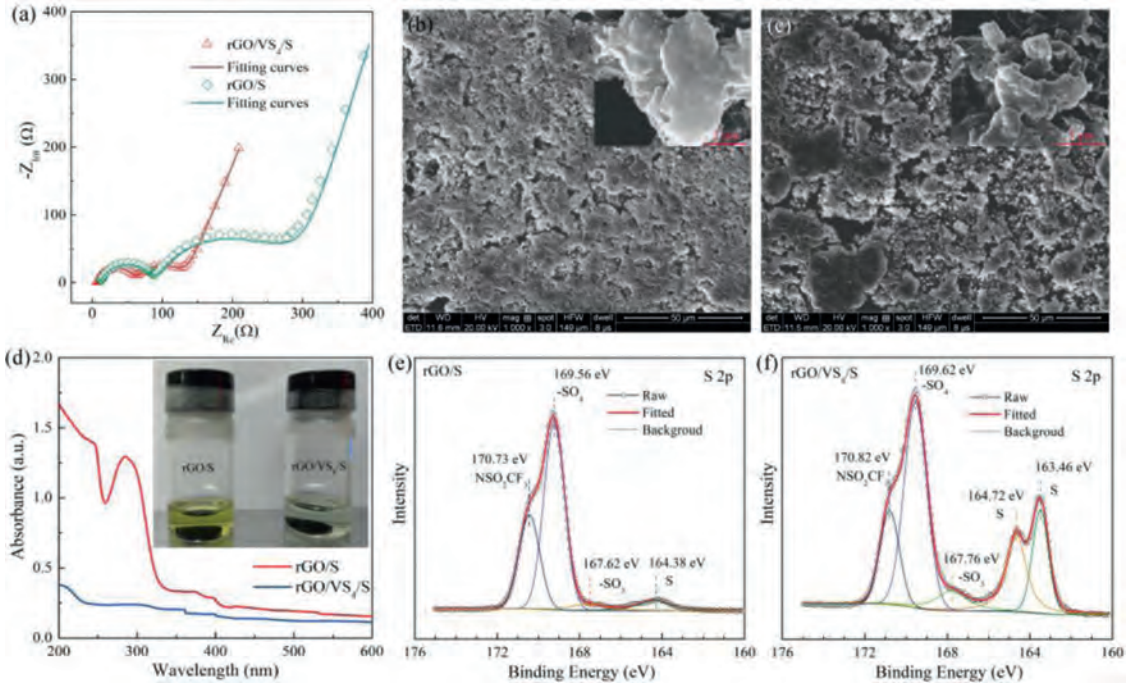

Fig. 4. (a) EIS and (b, c) SEM images of the charged rGO/S and rGO/VS_4/S electrodes after 100 cycles at 0.2 C. (d) UV–vis curves of solution adding the discharged rGO/S and rGO/VS_4/S electrodes after 100 cycles at 0.2 C, the inset image corresponds the soaking solution in DOL/DME. (e, f) XPS for the charged rGO/S and rGO/VS_4/S electrodes after 100 cycles at 0.2 C.

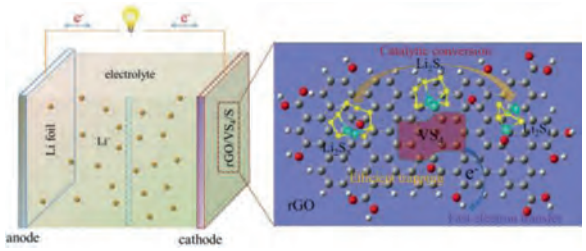

Fig. 5. Schematic illustration of promoted adsorption and the redox reactions of LiPS by rGO/VS_4 hosts.

mal method. Nanosized sulfur and VS_4 particles are uniformly distributed on the rGO matrix with benign contact. This obtained hybrid structure endows the merits of conductive rGO with physical anchoring effect and polar VS_4 with chemical adsorption and catalysis. Thus, the utilization of sulfur species and the electrochemical stability could be largely enhanced during the redox conversion. Typically, the potential difference at 0.1 C is decreased to 118 mV with a capacity of 1362 mAh/g. The capacity could maintain 82.3% from 1177 mAh/g to 969 mAh/g after 100 cycles at 0.2 C. The battery after long-term cycling (1000 cycles) delivers a reversible capacity of 548 mAh/g at 1 C with a capacity retention rate of 62.6%. The capacity fade rate is reduced to 0.0374% per cycle. Similarly, high-sulfur-loading Li–S battery with rGO/VS_4/S also exhibits favorable cycle stability and rate capability. This proposed one-step strategy to synthesize sulfur-based composites with multi-functional hosts could also be extended to prepare the active materials containing other sulfur hosts, which may provide a new and economical way to fabricate cathode materials for high-performance Li–S battery.

Declaration of competing interest

The authors declare no conflict of competing interest.

Acknowledgments

This work was supported by the National Natural Science Foundation of China (No. 21905289), the Independent Cultivation Program of Innovation Team of Ji'nan City (No. 2019GXRC011), the Natural Science Foundation of Shandong Province (No. ZR2020QE062), and China Postdoctoral Science Foundation (No. 2021T140268).

Supplementary materials

Supplementary material associated with this article can be found, in the online version, at doi:10.1016/j.cclet.2021.11.046.

References

[1] G. Harper, R. Sommerville, E. Kendrick, et al., Nature 575 (2019) 75–86.
[2] S. Chu, Y. Cui, N. Liu, Nat. Mater. 16 (2016) 16–22.
[3] J.B. Goodenough, Energy Environ. Sci. 7 (2014) 14–18.
[4] X.P. Gao, H.X. Yang, Energy Environ. Sci. 3 (2010) 174–189.
[5] R. Xu, Y. Sun, Y. Wang, J. Huang, Q. Zhang, Chin. Chem. Lett. 28 (2017) 2235–2238.
[6] A. Manthiram, Y.Z. Fu, S.H. Chung, C.X. Zu, Y.S. Su, Chem. Rev. 114 (2014) 11751–11787.
[7] Y.V. Mikhaylik, J.R. Akridge, J. Electrochem. Soc. 151 (2004) A1969–A1976.
[8] X.Q. Zhang, Y.L. Cui, Y. Zhong, et al., J. Colloid and Interf. Sci. 551 (2019) 219–226.
[9] S. Jiang, S. Huang, M. Yao, et al., Chin. Chem. Lett. 31 (2020) 2347–2352.
[10] T.T. Li, C. He, W.X. Zhang, J. Energy Chem. 52 (2021) 121–129.
[11] Z. Zhang, L.L. Kong, S. Liu, G.R. Li, X.P. Gao, Adv. Energy Mater. 7 (2017) 1602543.
[12] M.Y. Wang, X.H. Xia, Y. Zhong, et al., Chem. Eur. J. 25 (2018) 3710–3725.
[13] L. Luo, S.H. Chung, H.Y. Asl, A. Manthiram, Adv. Mater. 30 (2018) 1804149.
[14] X.J. Zhou, J. Tian, Q.P. Wu, J.L. Hu, C.L. Li, Energy Storage Mater. 24 (2020) 644–654.
[15] C.Y. Yang, N. Gong, T. Chen, et al., Green Energy Environ. (2021) doi:10.1016/j.gee.2021.03.001.
[16] X. Liu, J.Q. Huang, Q. Zhang, L.Q. Mai, Adv. Mater. 24 (2017) 1601759.
[17] Y.K. Wang, R.F. Zhang, J. Chen, et al., Adv. Energy Mater. 9 (2019) 1900953.
[18] L. Wang, Y.H. Song, B.H. Zhang, et al., ACS Appl. Mater. Interfaces 12 (2020) 5909–5919.
[19] B.A. Gao, X.X. Li, K. Ding, et al., J. Mater. Chem. A 7 (2019) 14–37.
[20] X. Chen, H.J. Peng, R. Zhang, et al., ACS Energy Lett. 2 (2017) 795–801.

[21] K. Xi, D.Q. He, C. Harris, et al., Adv. Sci. 6 (2019) 1800815.
[22] G.M. Zhou, H.Z. Tian, Y. Jin, et al., P. Natl. Acad. Sci. U.S.A. 114 (2017) 840–845.
[23] Z.B. Xiao, Z.L. Li, X.P. Meng, R.H. Wang, J. Mater. Chem. A 7 (2019) 22730–22743.
[24] J. Xu, T. Lawson, H.B. Fan, D.W. Su, G.X. Wang, Adv. Mater. 8 (2018) 1702607.
[25] X.J. Liu, N. Xu, T. Qian, et al., Small 13 (2017) 1702104.
[26] D.H. Liu, C. Zhang, G.M. Zhou, et al., Adv. Sci. 5 (2018) 1700270.
[27] M. Zhang, W. Chen, L.X. Xue, et al., Adv. Energy Mater. 10 (2019) 1903008.
[28] X. Liang, C.Y. Kwok, F. Lodi-Marzano, et al., Adv. Energy Mater. 6 (2016) 1501636.
[29] L. Wang, Z.Y. Wang, G.R. Li, S. Liu, X.P. Gao, Nano Energy 77 (2020) 105173.
[30] D. Cai, B.K. Liu, D.H. Zhu, et al., Adv. Energy Mater. 10 (2020) 1904273.
[31] X.Y. Tao, J.G. Wang, C. Liu, et al., Nat. Commun. 7 (2016) 11203.
[32] X.Y. Zhu, W. Zhao, Y.Z. Song, et al., Adv. Energy Mater. 8 (2018) 1800201.
[33] S.C. Wei, H. Zhang, Y.Q. Huang, et al., Energy Environ. Sci. 4 (2011) 736–740.
[34] C. Luo, Y.J. Zhu, O. Borodin, et al., Adv. Funct. Mater. 26 (2016) 745–752.
[35] Y.T. Liu, S. Liu, G.R. Li, T.Y. Yan, X.P. Gao, Adv. Sci. 7 (2020) 1903693.
[36] L. Huang, J.J. Li, B. Liu, et al., Adv. Funct. Mater. 30 (2020) 1910375.
[37] C.L. Chen, J.M. Jiang, W.J. He, et al., Adv. Funct. Mater. 30 (2020) 1909469.
[38] Z.Y. Wang, L. Wang, S. Liu, G.R. Li, X.P. Gao, Adv. Funct. Mater. 29 (2019) 1901051.
[39] R.Y. Fang, C. Liang, Y. Xia, et al., J. Mater. Chem. A 6 (2018) 212–222.
[40] Z.B. Cheng, Z.B. Xiao, H. Pan, S.Q. Wang, R.H. Wang, Adv. Energy Mater. 8 (2017) 1702337.
[41] L. Luo, S.H. Chung, A. Manthiram, J. Mater. Chem. A 6 (2018) 7659–7667.
[42] S.Z. Wang, H.Y. Chen, J.X. Liao, et al., ACS Energy Lett. 4 (2019) 755–762.
[43] L.Y. Zhu, C.S. Yang, Y.N. Chen, et al., J. Alloys Compd. 785 (2019) 855–861.
[44] G. Yang, B.W. Zhang, J.Y. Feng, et al., ACS Appl. Mater. Interfaces 10 (2018) 14727–14734.
[45] Y.L. Zhou, J. Tian, H.Y. Xu, J. Yang, Y.T. Qian, Energy Storage Mater. 6 (2017) 149–156.
[46] W.B. Li, J.F. Huang, L.Y. Cao, L.L. Feng, C.Y. Yao, Electrochim. Acta 274 (2018) 334–342.
[47] Z.Y. Li, B.P. Vinayan, P. Jankowski, et al., Angew. Chem. Int. Ed. 59 (2020) 11483–11490.
[48] Y.R. Wang, Z.T. Liu, C.X. Wang, et al., Adv. Mater. 30 (2018) 1802563.
[49] L. Luo, J.Y. Li, H.Y. Asl, A. Manthiram, ACS Energy Lett. 5 (2020) 1177–1185.
[50] M.N. Kozlova, Y.V. Mironov, E.D. Grayfer, et al., Chem. Eur. J. 21 (2015) 4639–4645.
[51] S. Britto, M. Leskes, X. Hua, et al., J. Am. Chem. Soc. 137 (2015) 8499–8508.
[52] S.H. Yu, X. Huang, K. Schwarz, et al., Energy Environ. Sci. 11 (2018) 202–210.
[53] Z. Zhang, D.H. Wu, Z. Zhou, et al., Sci. China Mater. 62 (2019) 74–86.
[54] S.Z. Wang, F. Gong, S.Z. Yang, et al., Adv. Funct. Mater. 28 (2018) 1801806.
[55] L. Kong, X. Chen, B.Q. Li, et al., Adv. Mater. 30 (2018) 1705219.
[56] Z. Yuan, H.J. Peng, T.Z. Hou, et al., Nano Lett. 16 (2016) 519–527.
[57] Y.Z. Song, W.L. Cai, L. Kong, et al., Adv. Energy Mater. 10 (2020) 1901075.
[58] L. Luo, S.H. Chung, C.H. Chang, A. Manthiram, J. Mater. Chem. A 5 (2017) 15002–15007.
[59] Y. Hu, W. Chen, T.Y. Lei, et al., Adv. Energy Mater. 10 (2020) 2000082.
[60] S. Jiang, S. Huang, M. Yao, et al., Chin. Chem. Lett. 31 (2020) 2347–2352.
[61] R. Li, Z. Bai, W. Hou, et al., Chin. Chem. Lett. 32 (2021) 3118–3122.
[62] X. Xu, S. Jeong, C. Sekhar Rout, et al., J. Mater. Chem. A 2 (2014) 10847–10853.
[63] W.J. Xue, Z. Shi, L.M. Suo, et al., Nat. Energy 4 (2019) 374–382.
[64] S.K. Liu, X.B. Hong, Y.J. Li, et al., Chin. Chem. Lett. 28 (2017) 412–416.
[65] S.I. Tobishima, H. Yamamoto, M. Matsuda, Electrochim. Acta 42 (1997) 1019–1029.
[66] D. Aurbach, E. Pollak, R. Elazari, et al., J. Electrochem. Soc. 156 (2009) A674–A702.
[67] X. Liang, C. Hart, Q. Pang, et al., Nat. Commun. 6 (2015) 5682.